AD NUMBER
AD318532
CLASSIFICATION CHANGES
TO: **UNCLASSIFIED**
FROM: **SECRET**
LIMITATION CHANGES
TO: **Approved for public release; distribution is unlimited.**
FROM: **Distribution authorized to U.S. Gov't. agencies and their contractors; Administrative/Operational Use; AUG 1960. Other requests shall be referred to Arnold Engineering Development Command, Arnold AFB, TN.**
AUTHORITY
E.O.11652 31 Dec 1970 (Doc Markings) ; AEDC ltr 31 Dec 1970

GENERAL DECLASSIFICATION SCHEDULE

IN ACCORDANCE WITH
DOD 5200.1-R & EXECUTIVE ORDER 11652

THIS DOCUMENT IS:

CLASSIFIED BY_____

Subject to General Declassification Schedule of Executive Order 11652-Automatically Downgraded at 2 Years Intervals- DECLASSIFIED ON DECEMBER 31, 1970

BY

Defense Documentation Center
Defense Supply Agency
Cameron Station
Alexandria, Virginia 22314

SECRET

SECRET

AEDC-TN-60-163

SECRET

(TITLE UNCLASSIFIED)

LONGITUDINAL STABILITY AND CONTROL CHARACTERISTICS OF A LENTICULAR MODEL AT MACH NUMBER 8

By

L. D. Kayser and M. E. Hillsamer
VKF, ARO, Inc.

August 1960

ARNOLD ENGINEERING DEVELOPMENT CENTER

AIR RESEARCH AND DEVELOPMENT COMMAND

US AF

SECRET

(Title Unclassified)

LONGITUDINAL STABILITY AND CONTROL CHARACTERISTICS OF A LENTICULAR MODEL AT MACH NUMBER 8

By

L. D. Kayser and M. E. Hillsamer
VKF, ARO, Inc

August 1960

ARO Project No. 341074
Contract No. AF 40(600)-800 S/A 11(60-110)

ABSTRACT

Aerodynamic force tests were conducted at a nominal Mach number of 8 on a lenticular model without and with four configurations of control surfaces. Data are presented for angles of attack up to 15 deg together with shadowgraphs of the flow around the model.

CONTENTS

ILLUSTRATIONS

NOMENCLATURE

MODEL NOMENCLATURE

A_b	Base area, 1.77 in.^{2}
S	Planform area of body, 153.94 in.^{2}
d	Body diameter, 14 in.
1 D	Body only
7 D.1	Body with twin tail surfaces in the body plane
7 D.2	Body with two control surfaces mounted at 15 deg
7 D.3	Model 7 D.1 with four 30-deg wedges attached
7 D.4	Body with four control surfaces, two mounted at + 15 deg and two mounted at -15 deg

COEFFICIENTS AND PARAMETERS

C_D	Forebody drag coefficient, $C_{D_t} - C_{D_b}$
C_{D_b}	Base drag coefficient, $-C_{p_b} \frac{A_b}{S} \cos \alpha$
C_{D_t}	Total drag coefficient, $\frac{\text{total drag}}{q_\infty S}$
C_L	Lift coefficient, $\frac{\text{lift}}{q_\infty S}$
C_{L_α}	Slope of lift curve, $(dC_L/d\alpha)_{\alpha = 0}$
C_m	Pitching-moment coefficient, $\frac{\text{pitching moment}}{q_\infty Sd}$
C_{m_α}	Slope of pitching-moment curve, $(dC_m/d\alpha)_{\alpha = 0}$
C_{p_b}	Base pressure coefficient, $\frac{p_b - p_\infty}{q_\infty}$

cp	Center of pressure, percent of body diameter from moment reference center
p	Pressure
q	Dynamic pressure
t	Temperature
α	Angle of attack

SUBSCRIPTS

b	Base conditions
∞	Free-stream conditions

INTRODUCTION

At the request of the Air Force Air Proving Ground Center, force tests on a lenticular model, without and with four configurations of control surfaces, were conducted in support of Air Force program Area 806A, Project 9860 at a nominal Mach number of 8 and a free-stream Reynolds number of 2.41×10^6 based on body diameter. The tests were performed in Tunnel B of the von Karman Gas Dynamics Facility, Arnold Engineering Development Center (VKF-AEDC) on May 25 and 26, 1960. The angle-of-attack range investigated was -15 to +15 deg. Shadowgraph pictures were obtained at 0 and 15-deg angle of attack. Representative results of the tests are presented.

APPARATUS

WIND TUNNEL

Tunnel B is an axisymmetric, continuous-flow, variable-density, hypersonic wind tunnel with a 50-in.-diam test section. The Mach 8 contoured nozzle produces an average test section Mach number, which varies from 8.02 at a stagnation pressure of 100 psia to 8.10 at 800 psia because of changes in boundary-layer thickness due to changing pressure level. The centerline flow distribution is uniform within about ±1 percent in Mach number, whereas off-center the flow is uniform to about ±0.3 percent. There is a slight axial gradient on the order of 0.01 Mach number per foot.

Details of Tunnel B and associated equipment are shown in Fig. 1. The hydraulically driven angle-of-attack sector pitches the model in a vertical plane from -15 to +15 deg with a straight sting. The remotely controlled, water-cooled, roll mechanism is electrically driven and is capable of rotating the model-sting combinations from -165 to +180 deg.

Stagnation pressures up to approximately 800 psia are supplied to Tunnel B by the VKF Compressor Plant. The air is selectively valved through the Compressor Plant, the high-pressure driers, and the propane-fired heater. The heater produces a maximum air temperature of 900°F, sufficient to prevent liquefaction of the air in the test section. From the heater, the air flows through the nozzle, the diffuser, the cooler, and back into the compressor system.

Manuscript released by authors August 1960.

MODELS AND SUPPORT

The basic body for all model configurations tested was a lenticular shape with a diameter of 14 in. and upper and lower surface radii of 25.27 in. The only surface irregularity was the balance and water-jacket housing. This basic body was designated configuration 1 D. Configuration 7 D.1 consisted of configuration 1 D with twin tail surfaces extending aft of the model and in the same plane as the body. The thickness of each tail at the rear was 0.25 in. and tapered forward at a total included angle of 1.1 deg. Configuration 7 D.2 consisted of the basic body with two controls mounted on the upper surface at 15 deg to the body plane. These controls had a minimum thickness of 0.25 in. and tapered forward at a total included angle of 9.0 deg. Configuration 7 D.3 (Figs. 2 and 3) was identical to configuration 7 D.1 except for the addition of four 30-deg wedges to the upper and lower surface of the aft portion of each tail. Configuration 7 D.4 (Figs. 4 and 5) was identical to configuration 7 D.2 except that two additional controls were added to the lower surface of the body and were placed at 15 deg to the body plane.

The model, water jacket, and balance were supported by a tapered sting with a half angle of 5.3 deg. The sting diameter at the aft end of the model was 1.12 in.

INSTRUMENTATION

A six-component, internal, strain-gage balance furnished by VKF was used to measure aerodynamic forces and moments on the models. The balance was designed for 30 lb axial force, ±100 lb normal and side force, ±350 in.-lb of pitching and yawing moment, and ±25 in.-lb rolling moment. Power to the strain-gage bridges was supplied by a 400-cps carrier system, and the outputs were measured with null-balance servo-potentiometers with shaft positioning digitizers for digital recording on punched paper tape.

The balance was cooled by a water jacket extending over the entire length of the balance. The forward end of the sting was also water cooled. Balance temperatures, measured by copper-constantan thermocouples, were monitored during the test.

Balance cavity and base pressures were measured with 5-psid Wiancko transducers referenced to about 500 microns of mercury. The reference pressure was measured with a Hastings vacuum gage and recorded by a manual input into the computer. The transducer outputs were measured with self-balancing potentiometers which converted the output to digital form.

DATA REDUCTION

An ERA 1102 digital computer was used for processing the raw data, which were automatically punched on paper tape by a high speed punch. The reduced data were tabulated by Flexowriter units.

PROCEDURE

Each of the five configurations was tested at a nominal Mach number of 8, a stagnation pressure of 480 psia, and a stagnation temperature of 900°F. These conditions correspond to a Reynolds number of 2.41×10^6 based on body diameter. Stagnation pressures and temperatures were measured at the instrument ring located (Fig. 1) upstream from the nozzle throat. Parameters, such as q_∞, p_∞, and t_∞, were calculated from the measured stagnation conditions with isentropic expansion through the nozzle assumed.

All configurations were tested in the pitch plane at zero deg angle of yaw. Data were obtained over the angle-of-attack range from -4 to+15 deg except for configuration 7 D. 2, which was tested from -15 to +15 deg.

The planform area (S) and diameter (d) of the basic body were used to reduce the data for all configurations. All coefficients were calculated with reference to the wind axes.

RESULTS AND DISCUSSION

Figures 6a-e give the static longitudinal stability and control characteristics of the five configurations tested. Figures 6a-c show the lift, drag, and pitching-moment coefficients as functions of angle of attack, whereas Fig. 6d shows the interdependence of lift coefficient and pitching-moment coefficient. Variation of center of pressure with angle of attack is shown in Fig. 6e. Values of cp at zero lift were obtained by using the ratio of the pitching-moment curve slope to that of the normal-force curve.

The basic lenticular model was longitudinally unstable about the moment reference point. Addition of control surfaces (configurations 7 D. 3 and 7 D. 4) produced longitudinal stability while increasing the drag and lift. The tail surfaces of configuration 7 D. 1 decreased the instability by a small factor; the effect on drag was negligible; and

the lift curve slope was slightly increased. The control surfaces of configuration 7 D. 2 decreased the instability of the basic model and maintained their effectiveness even at the large positive angles of attack when the surfaces were in the model wake. The lift curve slope for configuration 7 D. 2 was greater than for configuration 1 D, whereas the drag at the larger positive angles was essentially equal. Coefficients for configuration 7 D. 2 were very nearly equal to the coefficients for configuration 7 D. 4, assuming symmetry about the origin for configuration 7 D. 4 at the greater negative angles of attack.

Center of pressure, slope of the pitching-moment curve, and the lift-curve slope for configuration 1 D are presented in Fig. 7 as a function of Mach number. Data at Mach numbers other than Mach 8 were obtained in Tunnel A and Tunnel E-1 of VKF-AEDC (Refs. 1 and 2). Models tested in Tunnels E-1 and B had sharp edges, whereas the model tested in Tunnel A had an edge radius of 0. 004 d. The models were geometrically similar except for the edge radii. Extrapolation of Refs. 1 and 2 data compares favorably with data obtained in Tunnel B.

Figure 8 is a shadowgraph of configuration 7 D. 4 at $\alpha = 0$. The boundary layer is seen to be laminar over most of the model; however, the boundary layer became indistinguishable over the aft portion. Figure 9 is a shadowgraph of configuration 7 D. 2 at -15 deg angle of attack. The boundary layer on the lower surface appears to have separated and caused a weak shock wave to be formed. The boundary layer appears to have been laminar on the upper surface.

Additional information on other lenticular shapes can be found in Refs. 3 and 4.

REFERENCES

1. Anderson, A. "Force Tests of Lenticular Configurations at Supersonic Speeds." AEDC-TN-60-51, March 1960. (Secret)

2. Anderson, A. "Aerodynamic Test Results of Two Configurations of a Proposed Bomber Defense Missile at Supersonic Speeds." AEDC-TN-58-72, October 1958. (Secret)

3. Anderson, A. "Stability and Control Characteristics of Seven Lenticular Models at Mach Number 5." AEDC-TN-59-162, January 1960. (Secret)

4. Anderson, A. "Stability Tests of Three Lenticular Models at Supersonic Speeds." AEDC-TN-59-99, September 1959. (Secret)

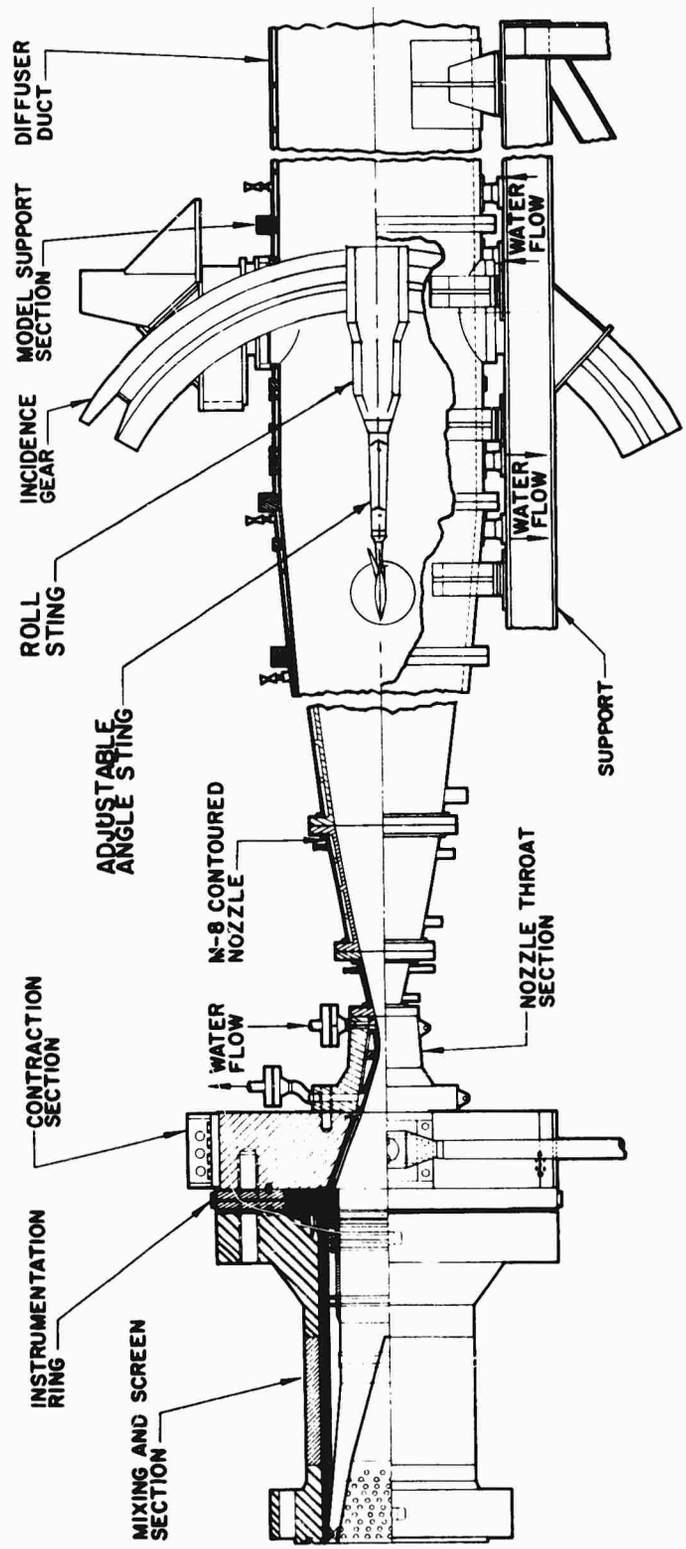

Fig. 1 General Layout, Tunnel B

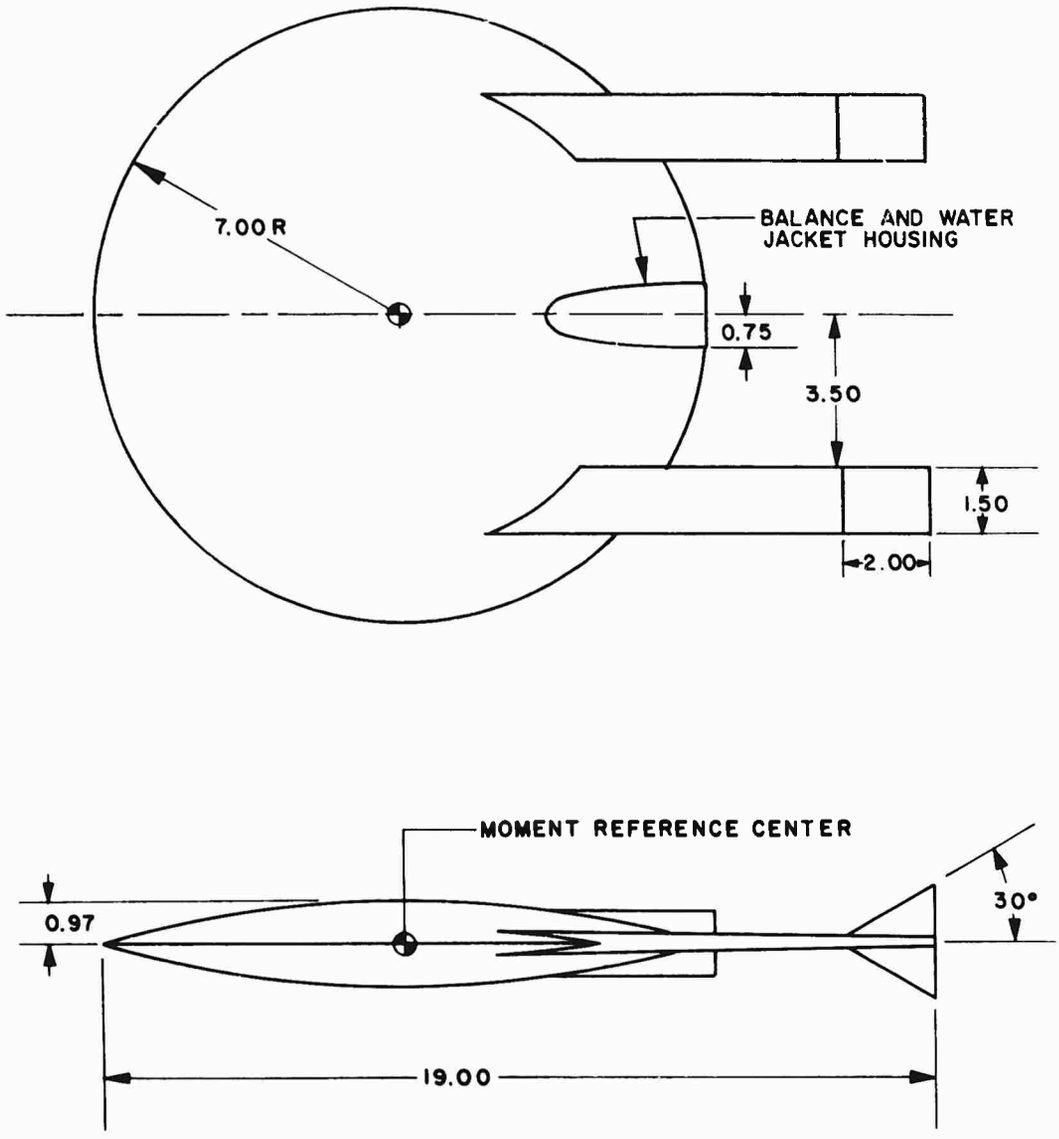

SURFACE RADIUS = 25.27

ALL DIMENSIONS IN INCHES

Fig. 2 Configuration 7 D.3 Geometry

Fig. 3 Configuration 7 D.3

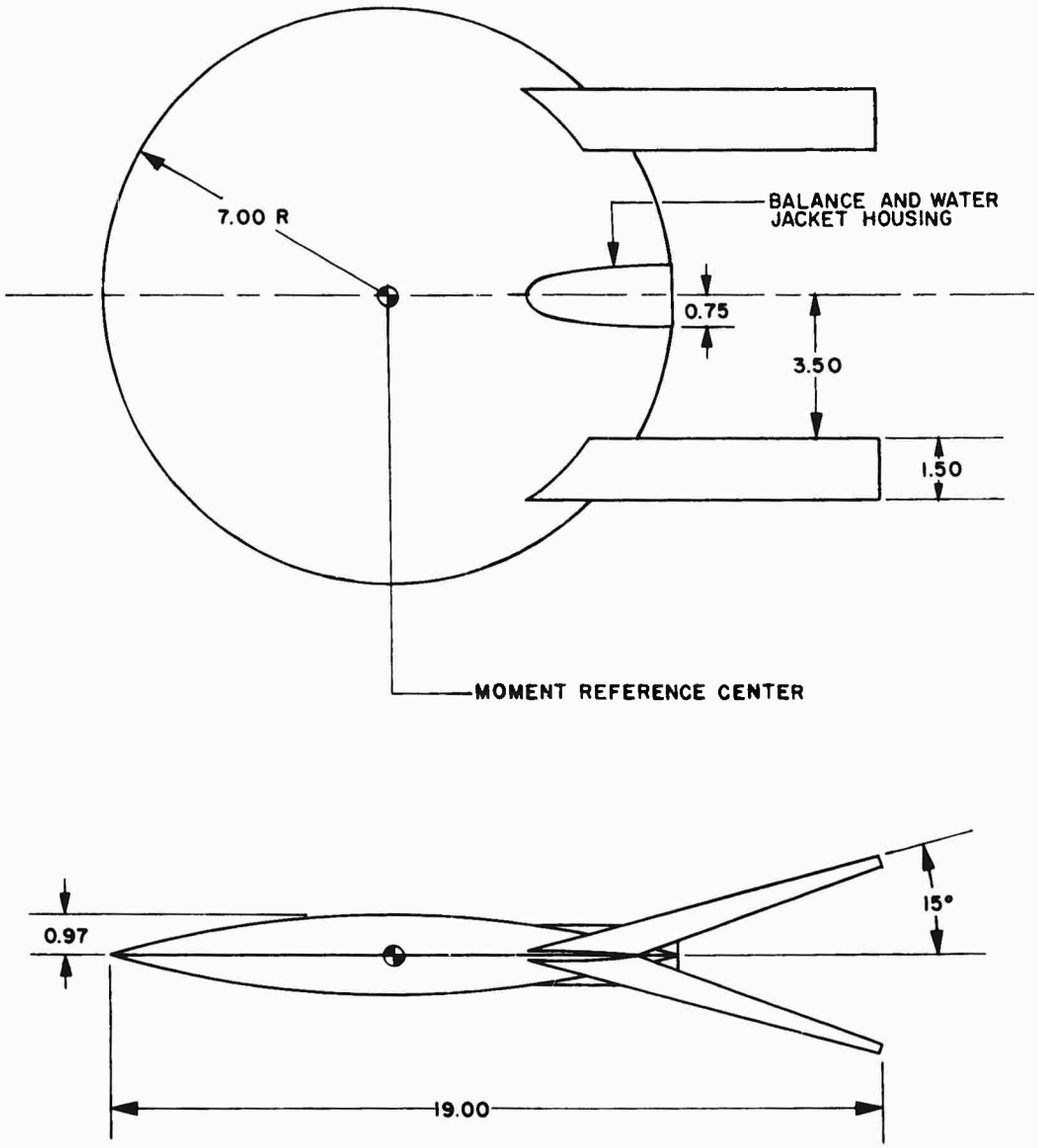

SURFACE RADIUS = 25.27
ALL DIMENSIONS IN INCHES

Fig. 4 Configuration 7 D.4 Geometry

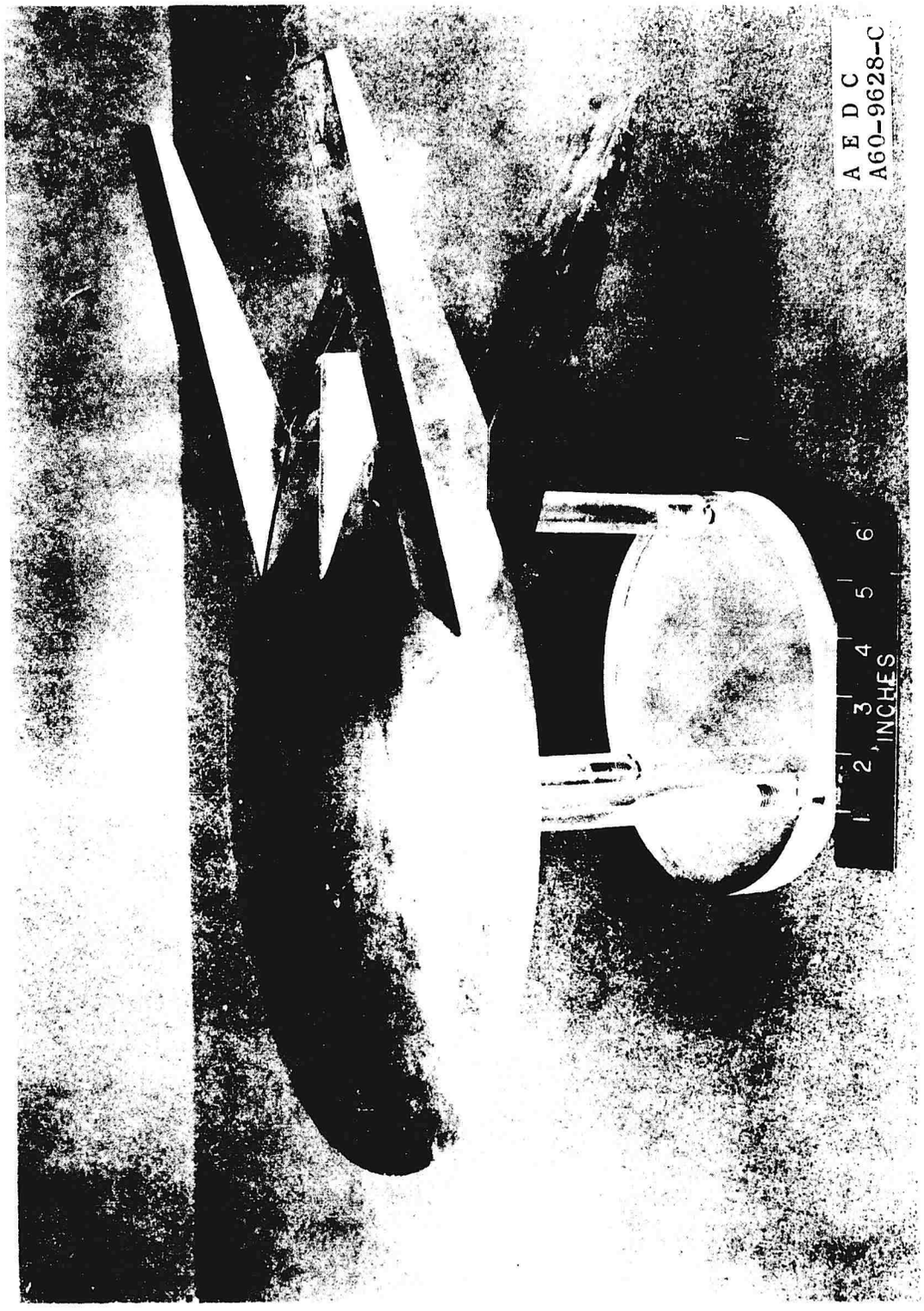

Fig. 5 Configuration 7 D.4

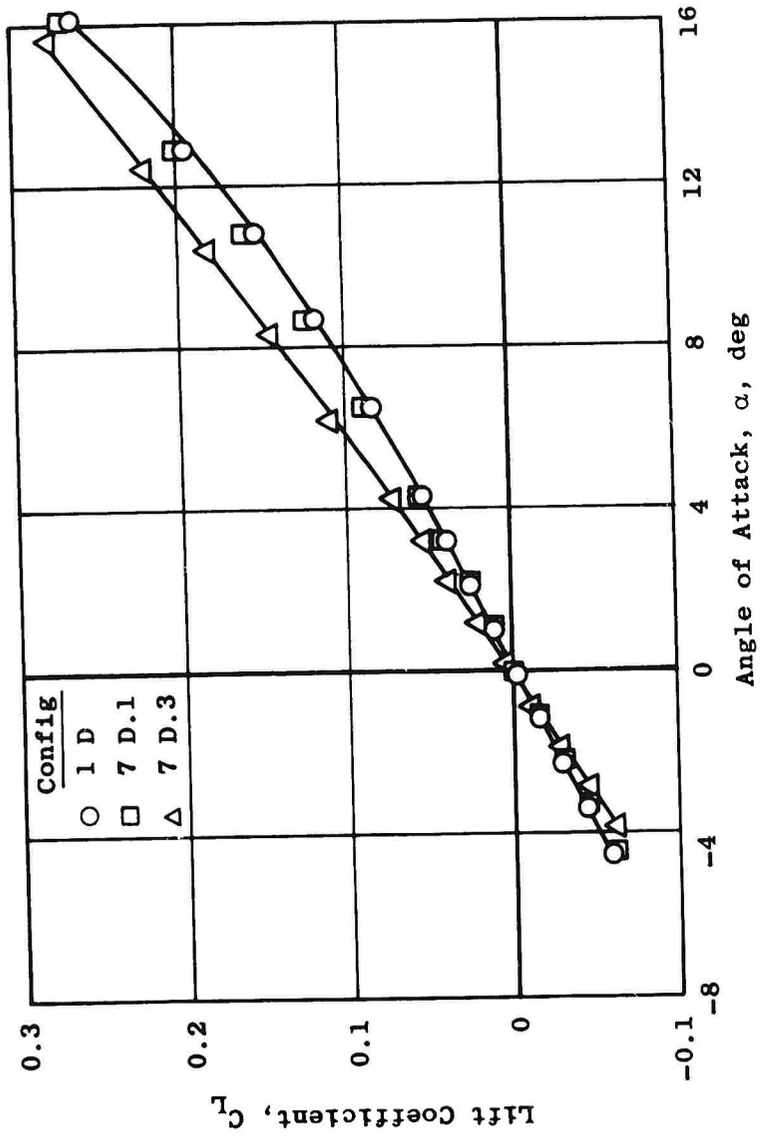

a. C_L vs α

Fig. 6 Effect of Control Surfaces on Aerodynamic Characteristics of the Configurations Tested

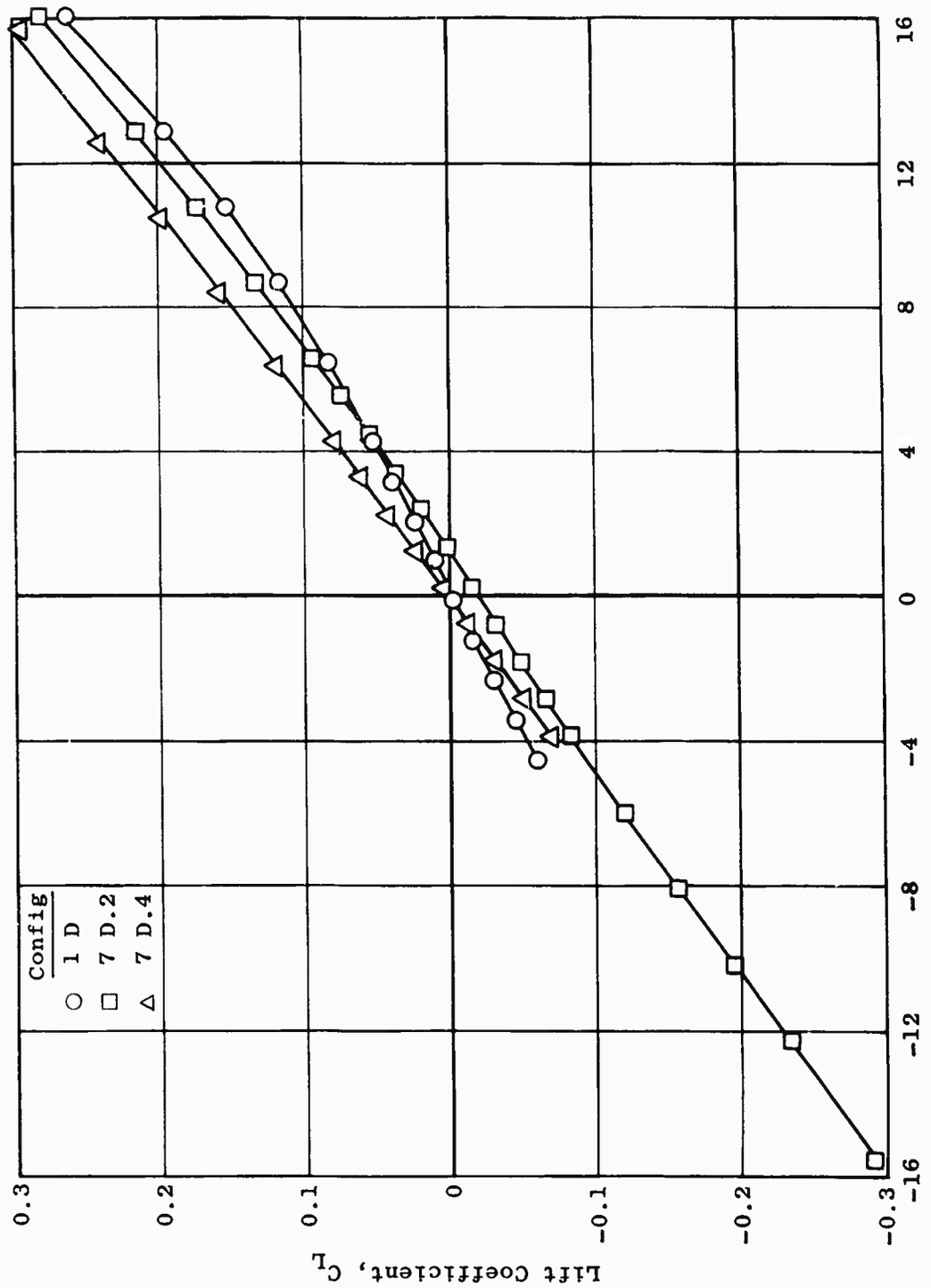

a. Concluded

Fig. 6 Continued

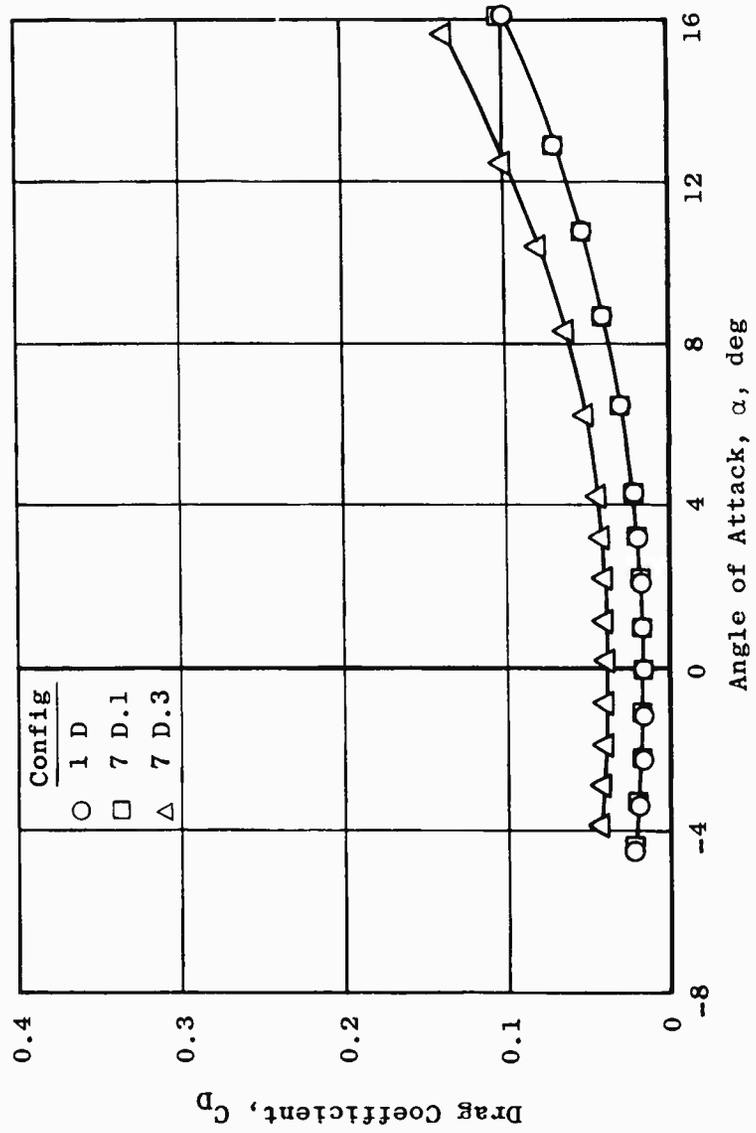

b. C_D vs α

Fig. 6 Continued

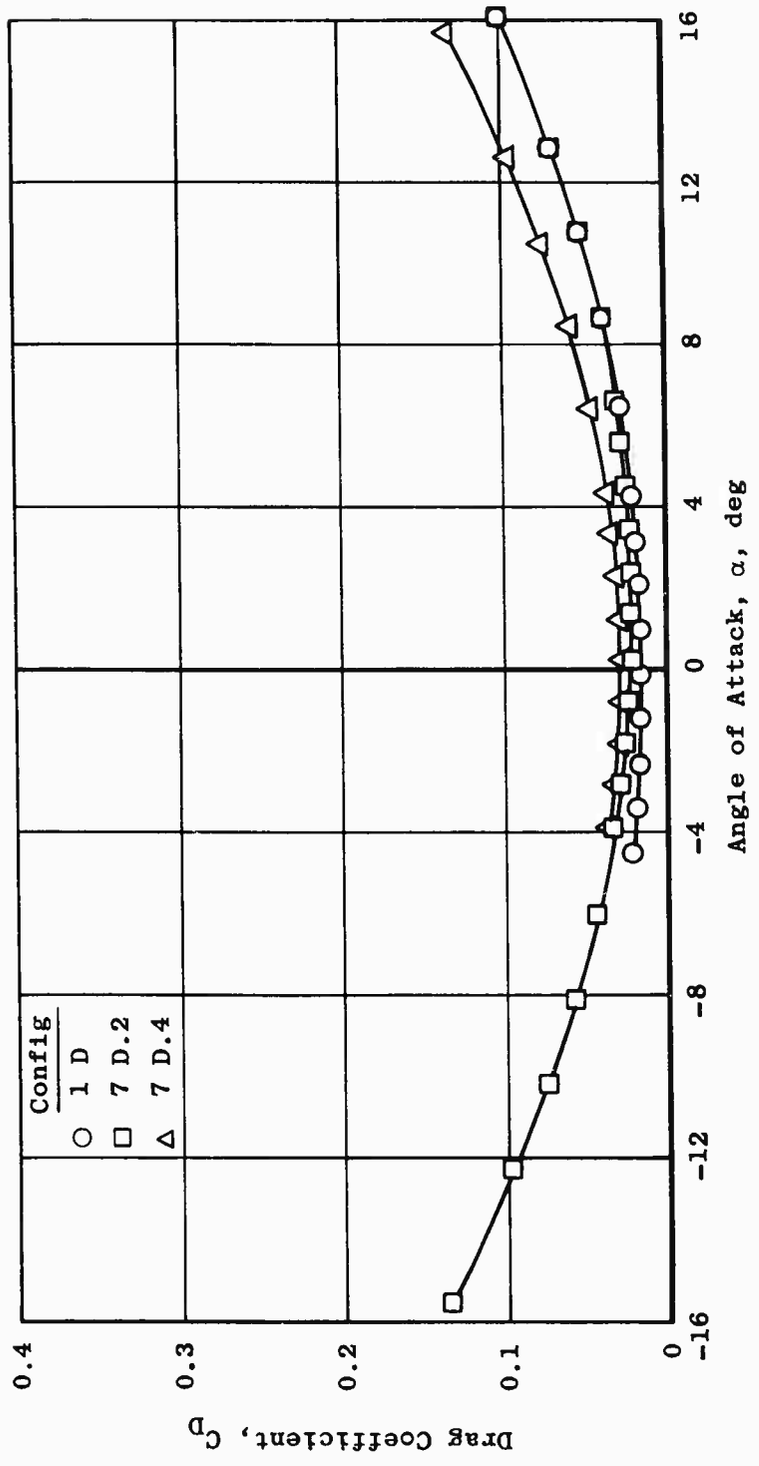

b. Concluded

Fig. 6 Continued

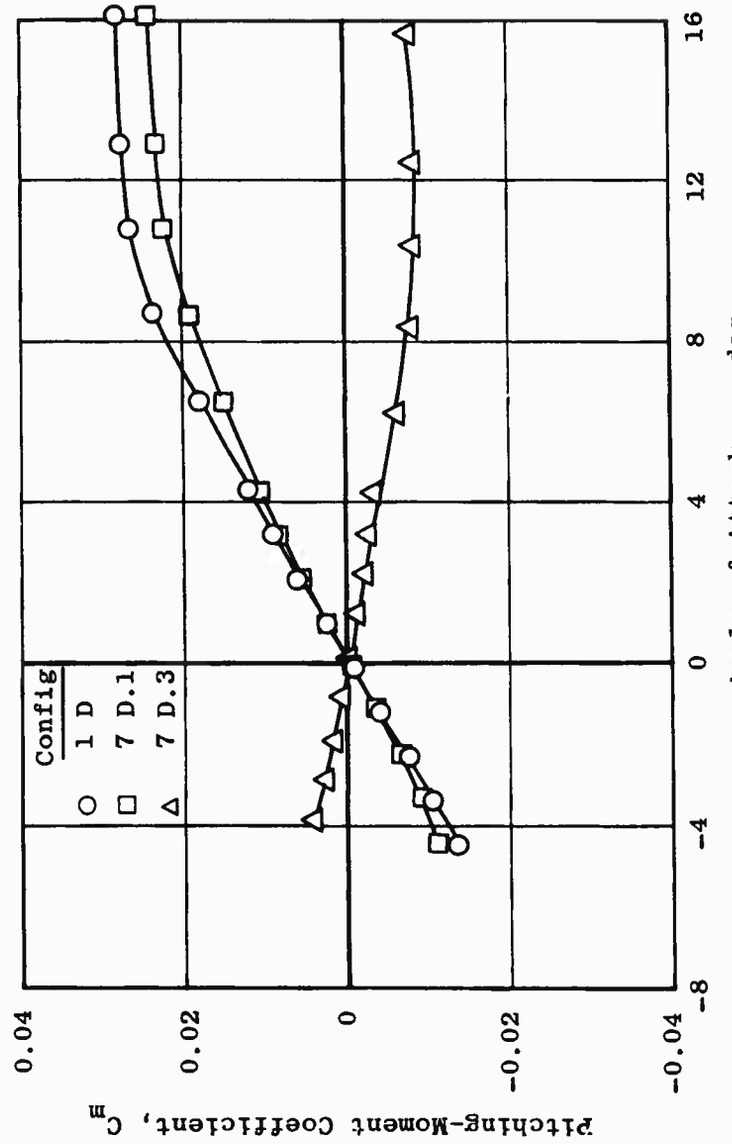

c. C_m vs α

Fig. 6 Continued

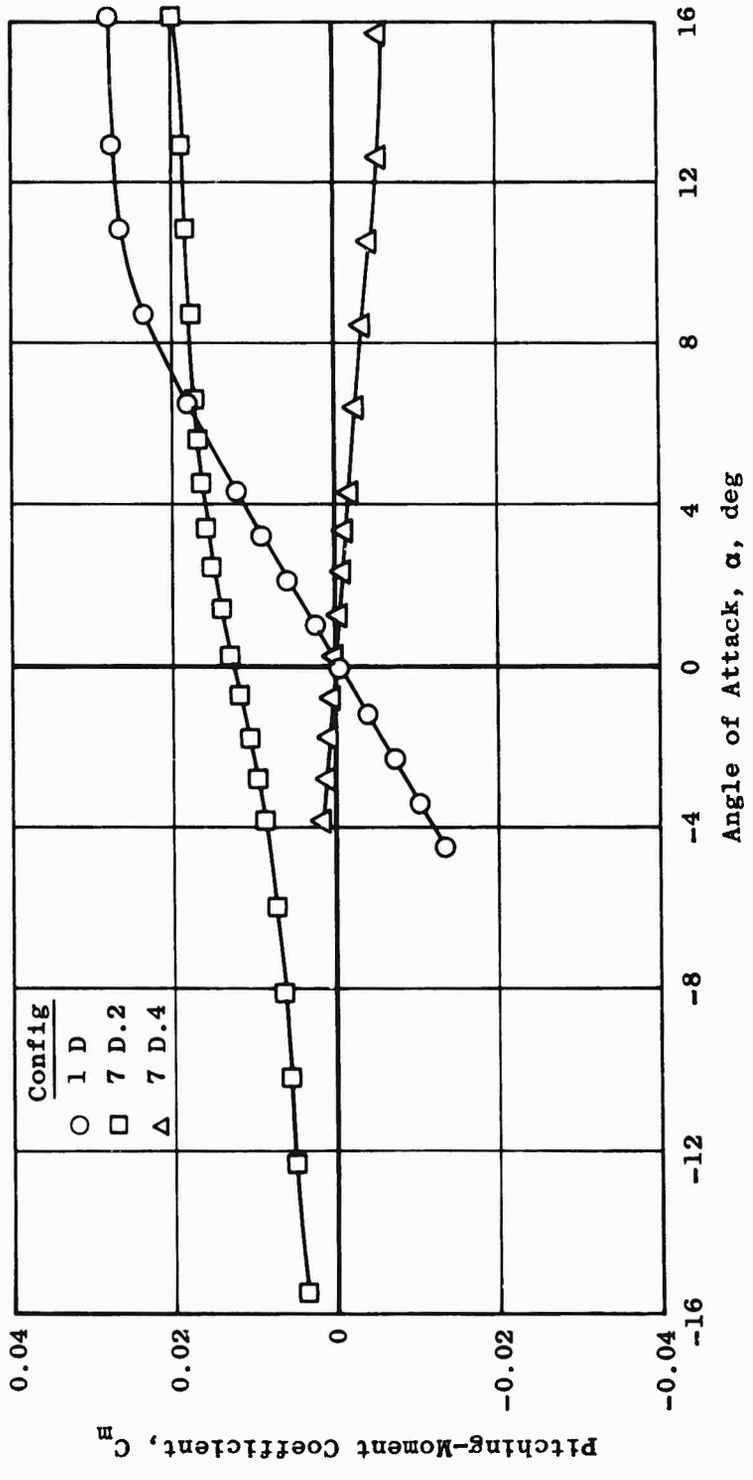

c. Concluded

Fig. 6 Continued

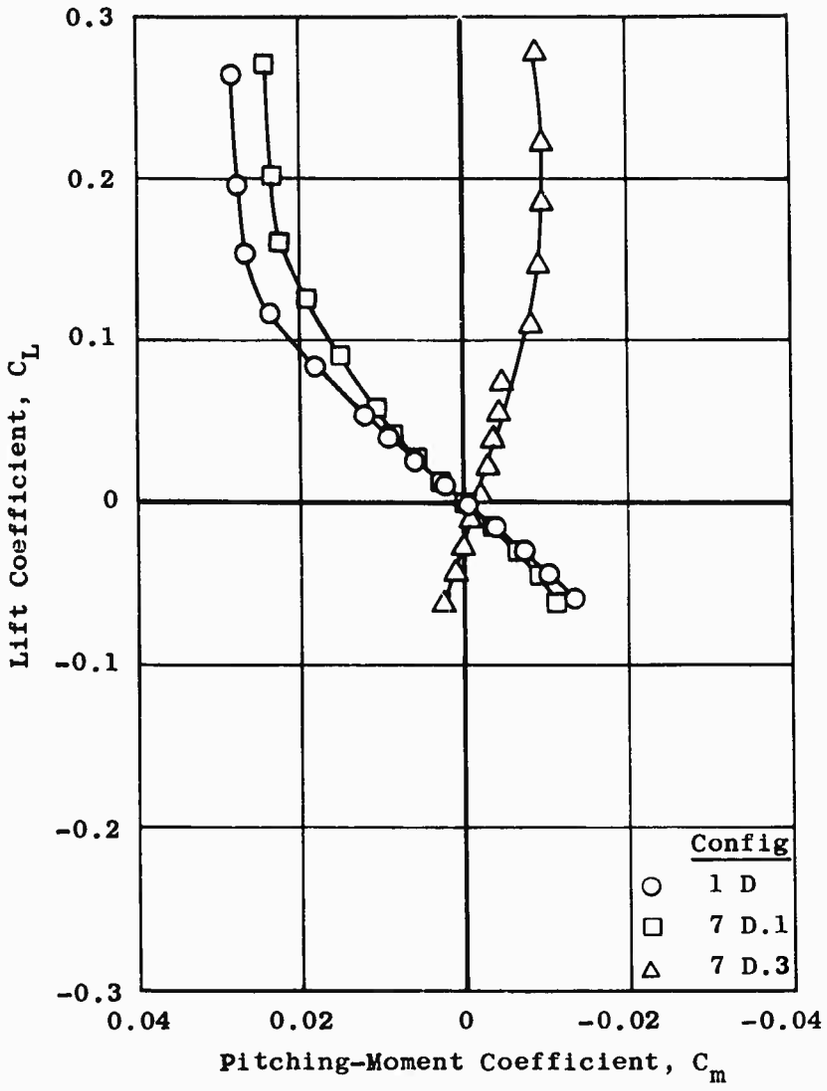

d. C_L vs C_m

Fig. 6 Continued

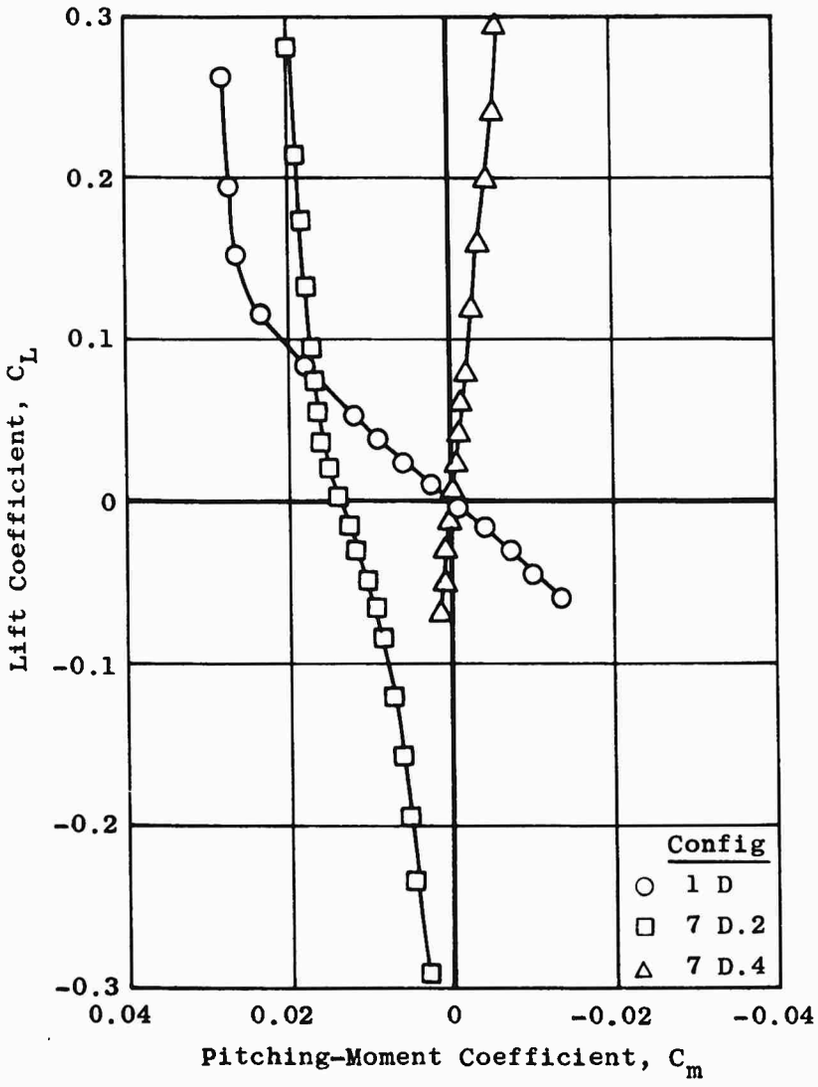

d. Concluded

Fig. 6 Continued

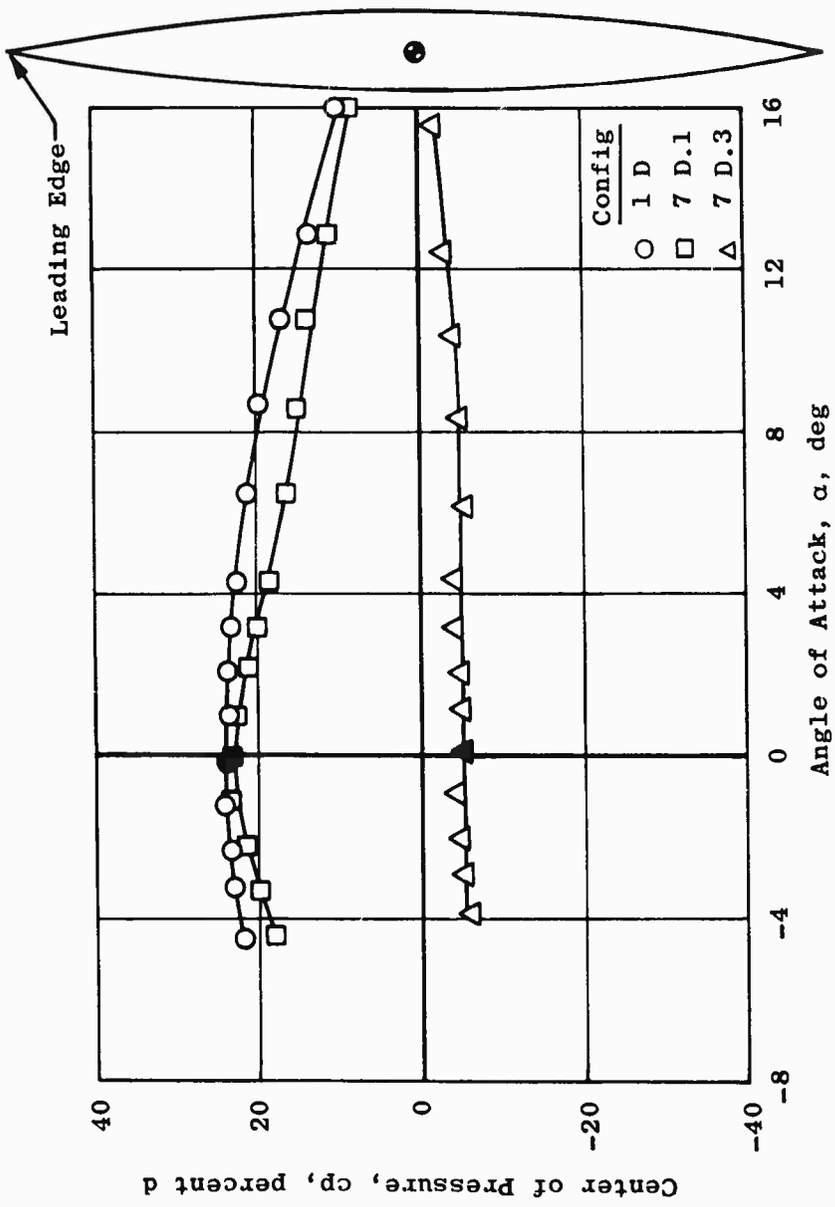

e. cp vs α

Fig. 6 Continued

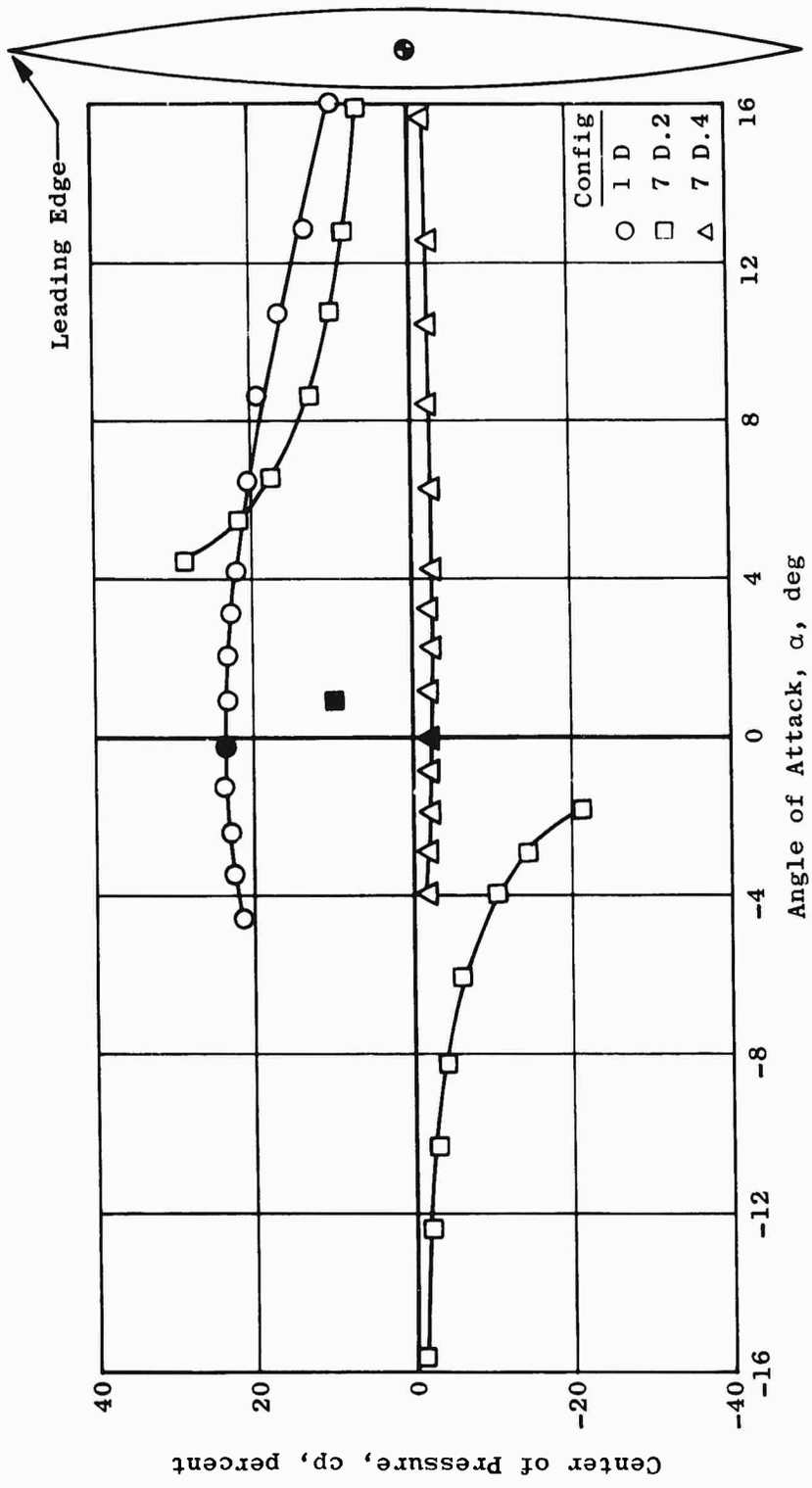

e. Concluded

Fig. 6 Concluded

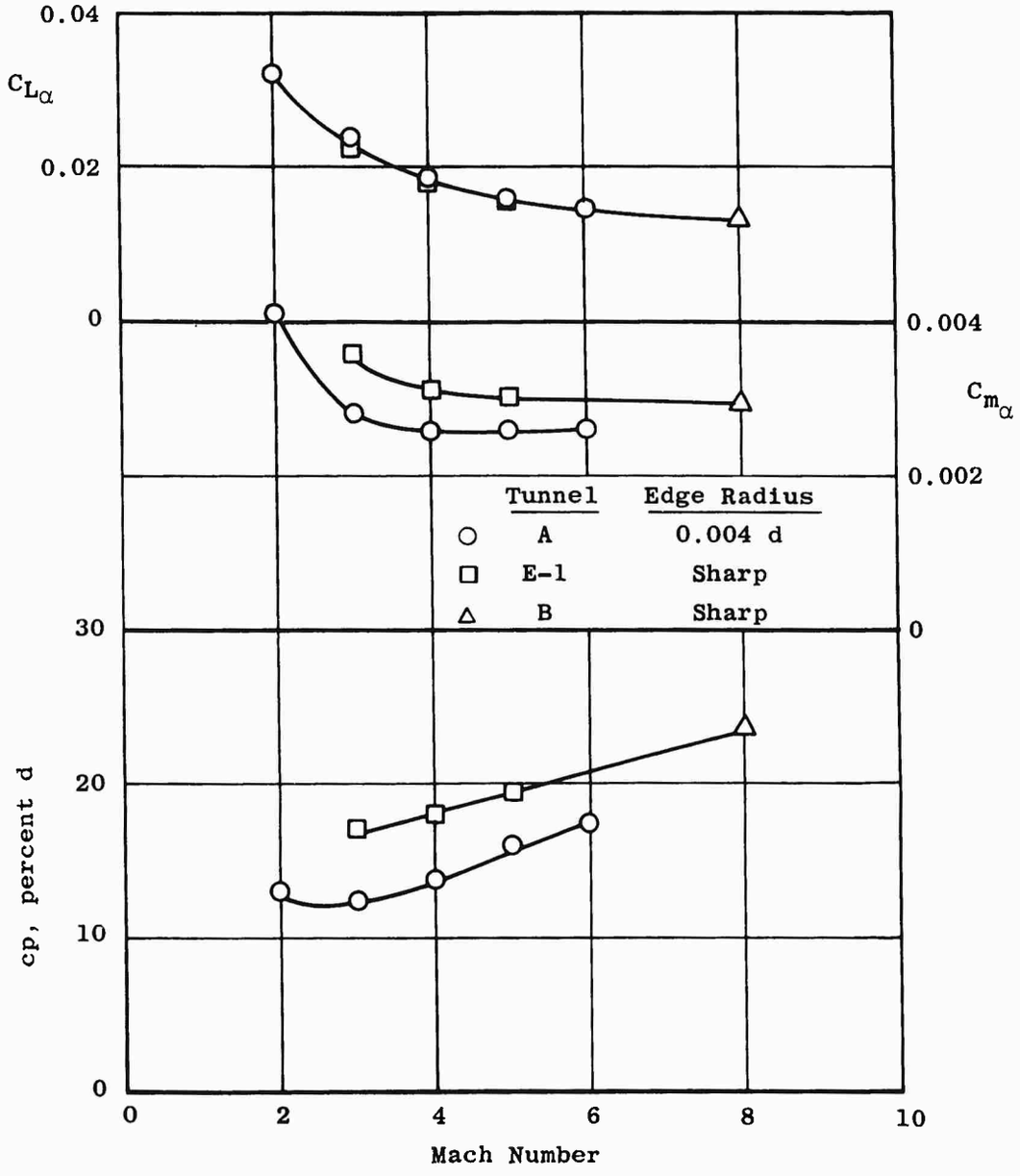

Fig. 7 Effect of Mach Number on C_L, C_m, and cp, Configuration 1 D

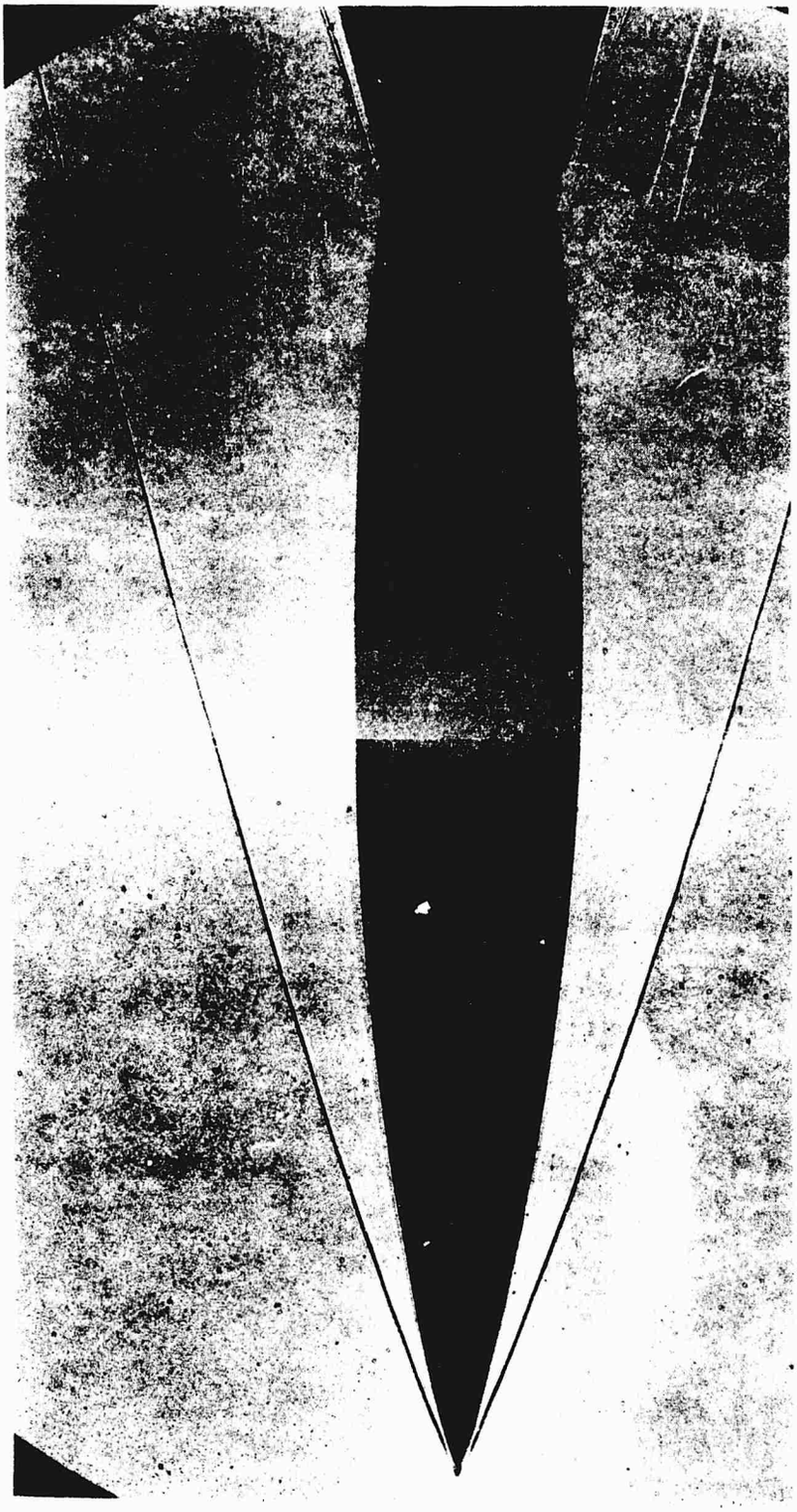

Fig. 8 Shadowgraph, Configuration 7 D.4, $\alpha = 0$

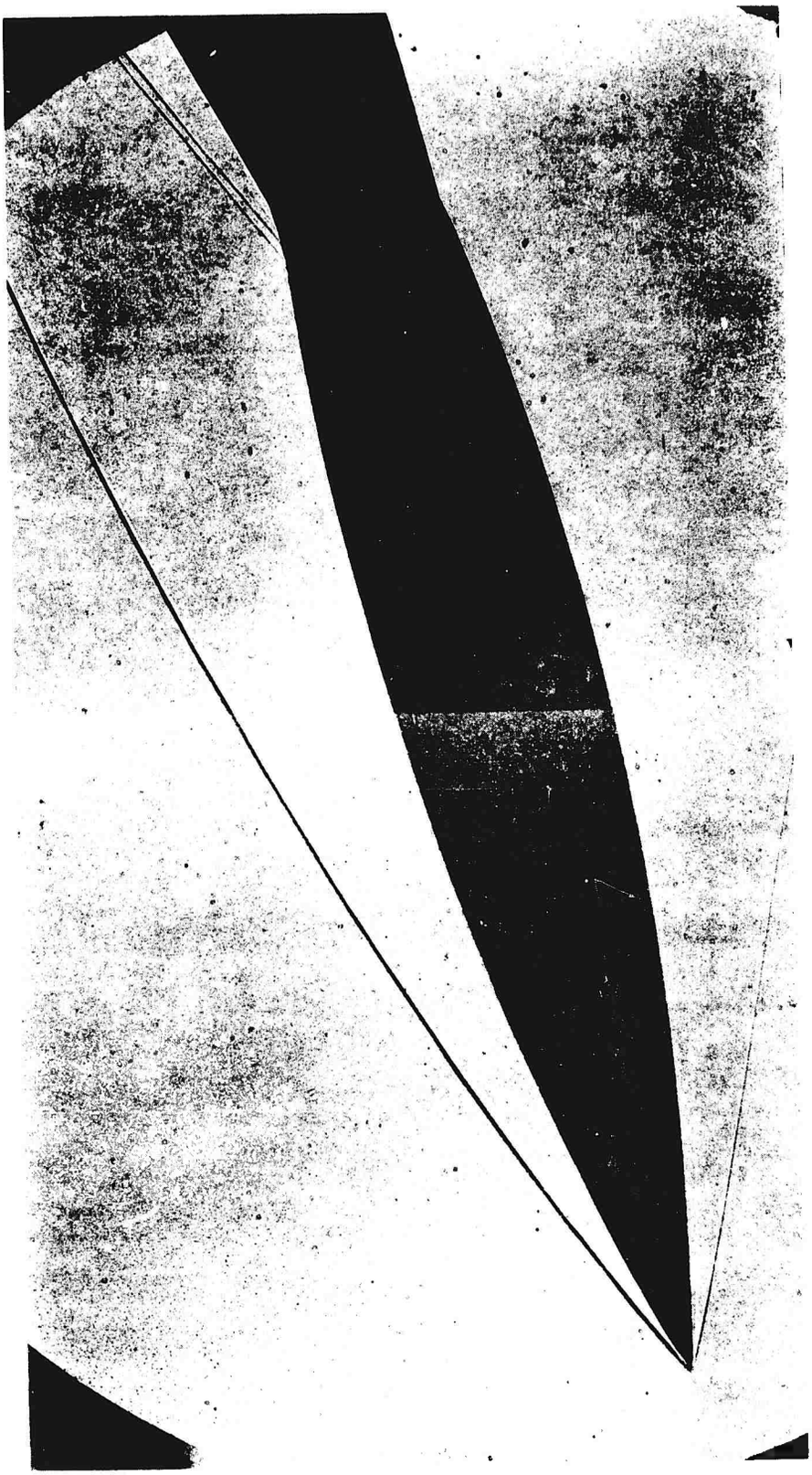

Fig. 9 Shadowgraph, Configuration 7 D.2, $\alpha = -15$